EFFECTS OF PASSIVE POROSITY ON INTERACTING VORTEX FLOWS AT SUPERSONIC SPEEDS

G. E. Erickson

Keywords: supersonic speeds, vortex flows, shock waves, schlieren, laser vapor screen, pressure-sensitive paint

ABSTRACT

A wind tunnel experiment was conducted in the NASA Langley Research Center (LaRC) Unitary Plan Wind Tunnel (UPWT) to determine the effects of passive surface porosity on vortex flow interactions about a general research fighter configuration at supersonic speeds. Optical flow measurement and flow visualization techniques were used and included pressure-sensitive paint (PSP), schlieren, and laser vapor screen (LVS). These techniques were combined with force and moment and conventional electronically-scanned pressure (ESP) measurements to quantify and to visualize the effects of flow-through porosity applied to a wing leading-edge extension (LEX) mounted to a 65° cropped delta wing model.

1 INTRODUCTION

The control of leading-edge vortex flows is a continuing challenge for designers of modern fighter aircraft. Passive porosity has been successfully applied to control vortices shed from slender bodies at subsonic through supersonic speeds [1] and to mitigate the adverse effects of shock waves on wings at transonic and supersonic speeds [2]. The present experimental investigation focuses on flow-through porosity to affect the vortex interactions for reduced nose-up pitching moments at supersonic speeds about a 65° cropped delta wing-LEX model. Porosity was applied to the LEX, since it is situated ahead of the moment reference center and generates a strong vortex flow that affects the wing flow field. A total of four configurations was tested and included non-porous (solid) and porous LEX in combination with centerline and wing-mounted vertical tails. Emphasis in the current paper is on the application of schlieren, LVS, and PSP techniques [3] to identify flow mechanisms and aerodynamic effects of LEX porosity.

2 TEST INFORMATION

2.1 Model and Instrumentation

A photograph of the 65° cropped delta wing-LEX model installed in the UPWT test section and an illustration of key dimensions of the model in terms of the fuselage station (F.S.) and butt line (B.L.) locations are included in fig. 1. The LEX was a flat-plate with beveled leading edge having a 65° sweep angle. It incorporated a pattern of 0.05-inch diameter through holes spaced 0.10 inch apart on center to provide a total porosity level of 12% relative to its exposed area. Testing of a solid LEX was accomplished by applying tape to the lower surface. An internal, 6-component strain-gauge balance was used to measure the model forces and moments. The model pitch attitude was determined using an accelerometer mounted in the main support system pitch mechanism with

corrections applied to account for tunnel flow angularity and aeroelastic deflections of the model/balance/sting assembly. The right-hand wing incorporated a total of 45 upper surface static pressure orifices distributed in three spanwise rows located at 30%, 60%, and 80% of the wing centerline chord measured aft from the apex of the wing (fig. 1). The pressure orifices were connected to an internal, 48-port, 10 psid ESP module with purge air capability, which allowed air to be routed through the pressure orifices during the PSP application process. The differential ESP module was used as an absolute gage by evacuating the reference side of the module using a vacuum source. The pressure data from the discrete pressure orifices were used to perform a global, in-situ calibration of the PSP intensity field images [3].

2.2 Optical Techniques

Schlieren and LVS flow visualization methods were used to obtain off-surface flow-field information. The UPWT test section is equipped with a single-pass, off-axis schlieren system that provides a two-dimensional image of the density gradients along the entire optical path. Shock waves and vortex flows are the primary flow field features visible in these images. The LVS system is used to visualize shock waves and vortices in cross planes. Water is injected into the wind tunnel circuit to create a fog in the test section, and the flow patterns about the model are illuminated by a sheet of laser light. The schlieren results are documented using still and video cameras located outside the test section, while the LVS flow visualization is recorded using cameras mounted inside the test section.

The PSP technique was used to acquire global surface static pressure distributions and intensity field images containing the signatures of vortices and shock waves. Optical access to the model is provided through windows in two doors which form the sidewalls of the test section. The model is rolled to a wings-vertical position during PSP testing, and the pitch angle is obtained using the model support system yaw mechanism. This setup limits the maximum angle of attack to approximately 8°. The PSP illumination source is provided by ultraviolet long-wave lamps, and images are acquired using scientific-grade, megapixel, digital cameras. Image processing is performed on a high-end computer workstation using the software package cited in [3].

2.3 Wind Tunnel and Test Conditions

The testing was conducted in the low Mach number test section of the NASA LaRC UPWT, which is a variable Mach number, variable-pressure, continuous-flow, supersonic wind tunnel. The test section dimensions are approximately 4 feet by 4 feet in cross section and 7 feet in length. A summary of the UPWT facility and testing capabilities is provided in [3]. Test results were obtained at free-stream Mach numbers of 1.6 and 2.1, Reynolds number of 2.0 million per foot, stagnation temperature of 125° Fahrenheit (F), and angles of attack from –4° to +22°. Dewpoint temperatures of approximately –30° F or less were maintained throughout the testing, except during the LVS portion of the experiment. The testing consisted of three phases because of conflicting data measurement, illumination, and image acquisition requirements: (1) force, moment, and ESP pressure measurements and schlieren flow visualization through the complete ranges of Mach number and angle of attack; (2) LVS flow visualization at selected test conditions and model cross-flow locations; and (3) PSP image acquisition at selected combinations of Mach number and angle of attack.

3 DISCUSSION OF RESULTS

3.1 Force and Moment Measurements

LEX porosity causes large, nose-down increments to the pitching moment coefficient. Concurrent effects include lower lift and higher drag at the moderate and high angles of attack. Test results are shown in fig. 2 corresponding to Mach=2.1, which are typical of the trends observed at lower

Mach number. The force and moment data suggest that porosity weakens the LEX vortex and, consequently, decreases the vortex-induced lift and pitching moment increments. The increased drag is attributed to the flow through the porous surface.

3.2 Schlieren Flow Visualization

Figs. 3 and 4 present schlieren flow visualization results obtained with the solid and porous LEX at Mach=1.6, α=10° and Mach=2.1, α=16°, respectively. The vortex flows are visible in the schlieren images as lighter regions extending nearly streamwise above the model surface. Porosity causes a diffusion of these lighter regions, which is consistent with a weakening of the vortex shed from the LEX. The LEX vortex is not suppressed by porosity, since vorticity is still shed from the LEX leading edge, albeit to a lesser degree.

3.3 Laser Vapor Screen Flow Visualization

The effect of porosity on the LVS cross-flow pattern at Mach=1.6, α=8° and the 80% wing chord station (x/c=0.80) is shown in fig. 5. The light sheet location corresponds to the aft ESP pressure tap row on the right-hand wing upper surface, and the test conditions also coincide with PSP results discussed in the next section. Porosity shifts the dominance from the LEX vortex to the wing vortex. The solid LEX image is highlighted by two distinct vortex pairs, which are revealed as darker regions lacking condensate. The left- and right-hand LEX vortices have nearly circular cross sections and are positioned along the inboard portion of the wing. A region of intense downflow is induced between these vortices. The left- and right-hand wing leading-edge vortices are flatter regions situated along the outer section of the wing. In contrast, the porous LEX image reveals one vortex pair featuring a broader, thicker wing leading-edge vortex on each side. There is no evidence of the LEX vortices, and the induced downflow above the fuselage is less discernible.

The cross-flow pattern at the same light sheet location at Mach=2.1 is shown in figs. 6 and 7 corresponding to α=12° and 16°, respectively. The weaker vortex produced by the porous LEX combines with the wing leading-edge vortex, and the shear layer from the wing leading edge connects the two vortices. The bulk of this vortex region is situated closer to the wing surface, which would suggest a local increase in the vortex-induced surface pressures. This pattern is more consistent with the schlieren results in fig. 4, which revealed vortex traces starting at the LEX and extending along the entire wing. The identities of the LEX and wing vortices can still be discerned, but the resultant cross flow pattern is characteristic of a single, broader vortical flow. Consistent with this effect is the development of a single cross-flow shock above the combined vortex region, in contrast to the separate shocks that develop above the LEX and wing vortices in the solid LEX images.

3.4 PSP Intensity Field Images

3.4.1 Centerline versus Twin Tails

Several PSP formulations were evaluated during the current experiment, and the most complete image base was acquired on the model with twin tails using a more recent and robust PSP chemistry and base coat described in [3]. The schlieren and vapor screen images previously shown correspond to the model with the centerline tail. The centerline and twin tails are positioned downstream of the 80% wing chord station and, consequently, their upstream influence at supersonic speeds is limited to disturbances transmitted through the wing boundary layer. As a result, the vortex-dominated flow field forward of the tail positions is similar for both tail arrangements. This is confirmed in fig. 8, which shows the PSP intensity field images for the solid LEX with the centerline tail and twin tails, obtained using different PSP formulations, at Mach=1.6 and α=8°. PSP coating was not applied to the LEX, and this surface does not appear in the images. The lower pressure regions underneath the vortical flows are denoted by the blue/purple colors, while higher pressure regions downstream of shock waves or in areas of vortex-induced reattached

flow are denoted by the red/pink colors. The surface pressure field in these fully processed and calibrated images compare favorably in the region of the wing upstream of the tail positions, and differences are noted only in the local region about the tails. The intensity field response to the LEX vortex is faint compared to the wing vortex, despite its dominance in the schlieren and vapor screen images, because it is situated higher above the wing surface. The primary effect of the LEX vortex is indirect and is manifested in the size, strength, and location of the wing vortical flow.

3.4.2 Solid versus Porous LEX

Fig. 9 compares the PSP intensity field images obtained on the twin-tail configuration at Mach=1.6 and α=8° with the solid and porous LEX. The porous LEX image features a single, broader wing vortex footprint, which correlates with the vapor screen image at the same test conditions in fig. 5. The weaker flow components induced by the LEX vortex on the wing allow a forward migration of the wing vortex origin towards the LEX-wing junction. Porosity also alleviates the region of higher pressure near the wing apex which was associated with the downflow and subsequent flow reattachment induced by the vortex from the solid LEX. The sweep of the shock waves created at the twin tails is reduced with the porous LEX, which suggests a decrease in the vortex-induced spanwise flow component in this region of the wing.

The effect of porosity on the PSP intensity field is unaffected by increased Mach number, as indicated in the PSP images in fig. 10 at Mach=2.1 and α=8°. A slight broadening of the wing vortex footprint is apparent, which is an expected result at the higher Mach number.

3.5 PSP Pressure Distributions

3.5.1 In-Situ Calibrations

The locations of the ESP pressure taps provided discrete pressure measurements that adequately covered the expected range of pressures in the current experiment. As a result, the in-situ calibration method provided an excellent global calibration of the PSP. An example of the good agreement between the two measurement techniques is shown in fig. 11, which compares the PSP and ESP spanwise distributions of the upper surface static pressure coefficient (CPU) plotted as a function of nondimensional span location (y/s) at x/c=0.60 and x/c=0.80, Mach=1.6, and α=8°.

3.5.2 Centerline versus Twin Tails

Quantitative confirmation of the similarity of the wing flow field upstream of the centerline and twin vertical tails is provided in the PSP pressure distributions at Mach=1.6 and α=8° in fig. 12. The results at x/c=0.60 and x/c=0.80 were obtained from the corresponding intensity field images shown previously in fig. 8.

3.5.3 Solid versus Porous LEX

Figs. 13 and 14 show the effect of porosity on the PSP pressure distributions at Mach=1.6 and 2.1, respectively, and α=8°. The dual vortex pressure signatures characteristic of the solid LEX configuration are contrasted by the single, broader signature associated with the porous LEX. Porosity typically causes a slight reduction in the suction pressures along the outer wing region, but this effect is offset by an inboard region of higher suction pressures which act over an effectively larger portion of the wing. This trend occurs at both pressure measurement stations and Mach numbers and is consistent with the redistribution of the vortex cross-flow patterns in the vapor screen images. These results suggest that the redistribution of the wing vortex-induced suction pressures counters the decreased direct lift on the LEX, except at the higher angles of attack, and contributes to the nose-down pitching moment increments shown previously in fig. 2.

3.5.4 Mach Number Effect

Figs. 15 and 16 show the effect of the Mach number on the PSP pressure distributions at α=8° for the solid and porous LEX, respectively. Increasing the Mach number from 1.6 to 2.1 weakens the vortical flows and causes a reduction in the vortex-induced suction pressure levels. However, the character of the pressure distributions, and the effect of porosity, are unaffected by the Mach number.

4 SUMMARY

Optical measurement and flow visualization techniques were used to identify the effects of passive porosity to control the interacting vortex flows about a 65° cropped delta wing-LEX configuration at supersonic speeds. Flow-through porosity applied to the LEX reduced the nose-up pitching moments that are characteristic of a LEX vortex-dominated flow field. Schlieren and LVS flow visualizations indicated that porosity promoted a wing vortex-dominated flow field as a result of a diffusion and weakening of the LEX vortex. The LVS and PSP results obtained with the porous LEX revealed a single, broader wing vortical flow. The redistribution of the wing vortex-induced suction pressures contributed to the nose-down pitching moment increments and mitigated the decrease in the LEX vortex-induced lift, except at the higher angles of attack. The schlieren, LVS, and PSP techniques were mutually exclusive because of conflicting illumination and image acquisition requirements. However, the combined results from these optical methods provided a more complete assessment of the effects of passive porosity on the high angle-of-attack flow field.

REFERENCES

[1] Bauer S. X. S. and Hemsch M. J.: Alleviation of Side Force on Tangent-Ogive Forebodies Using Passive Porosity. AIAA 10th Applied Aerodynamic Conference, Palo Alto, CA, AIAA-92-2711, June 22-24, 1992.

[2] Bauer S. X. S. and Hernandez G.: Reduction of Cross-Flow Shock-Induced Separation with a Porous Cavity at Supersonic Speeds. AIAA 6th Applied Aerodynamics Conference, Williamsburg, VA, AIAA-88-2567, June 6-8, 1988.

[3] Erickson, G.E.: Overview of Selected Measurement Techniques for Aerodynamics Testing in the NASA Langley Unitary Plan Wind Tunnel. AIAA Fluids 2000 Conference, Denver, CO, AIAA 2000-2396, June 19-22, 2000.

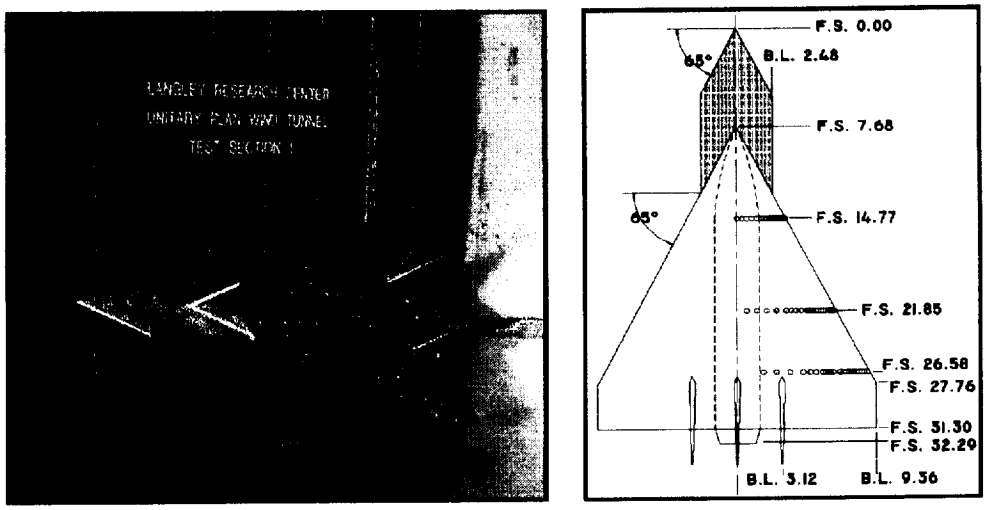

Fig. 1. Installation photograph and details of porous LEX model

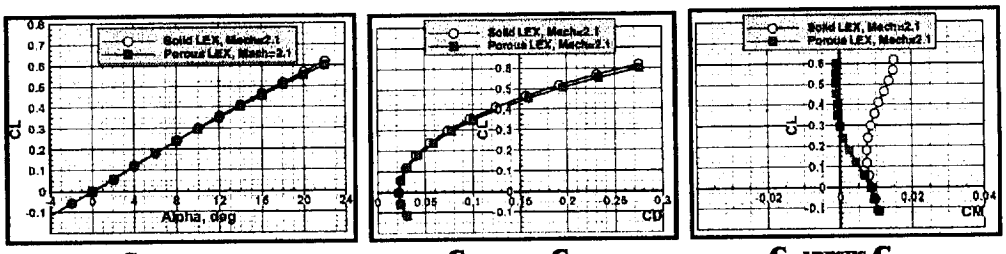

C_L versus α C_L versus C_D C_L versus C_m

Fig. 2. Porosity effect on lift, drag, and pitching moment coefficients at Mach=2.1

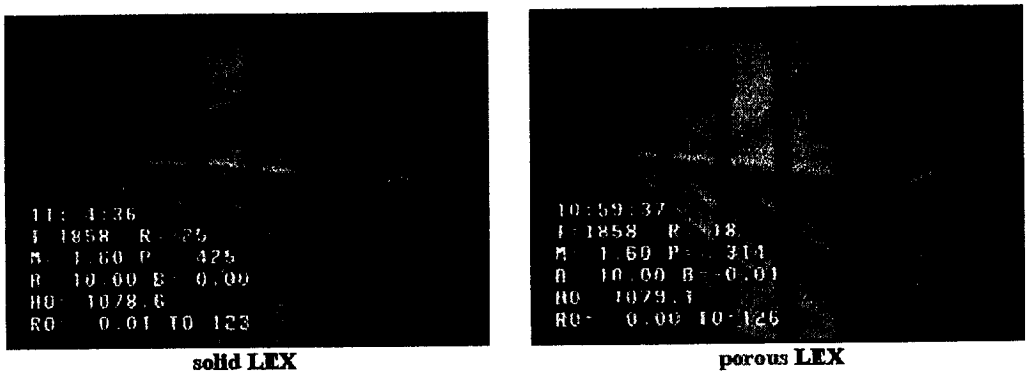

solid LEX porous LEX

Fig. 3. Schlieren flow visualization of solid and porous LEX configurations at Mach=1.6, α=10°

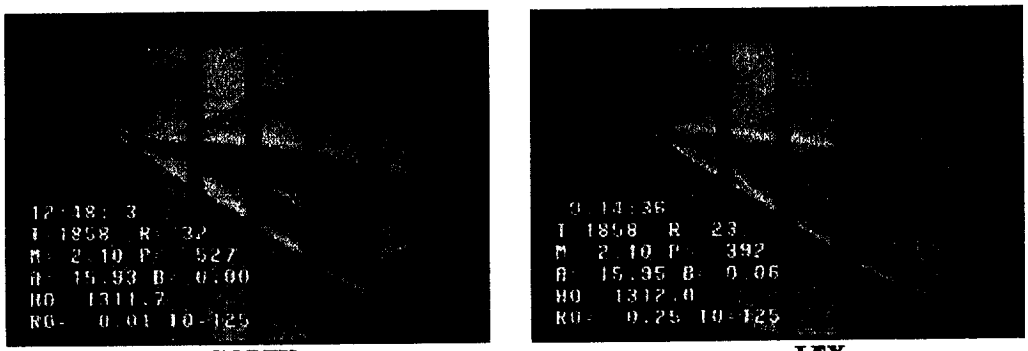

solid LEX porous LEX

Fig. 4. Schlieren flow visualization of solid and porous LEX configurations at Mach=2.1, α=16°

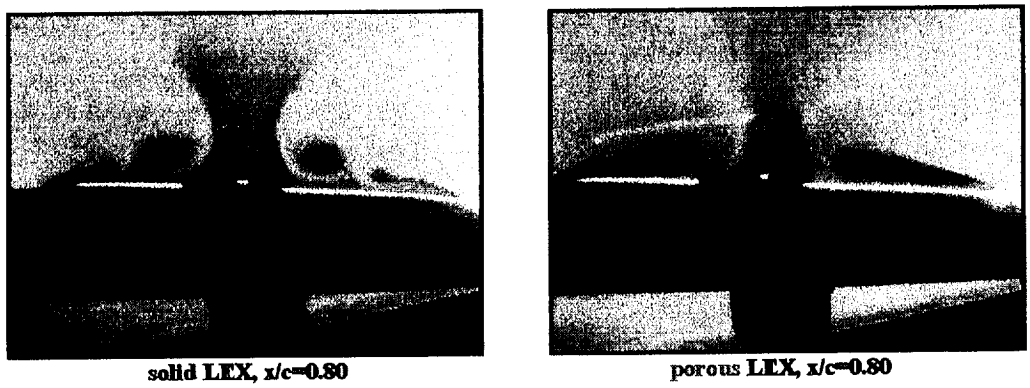

solid LEX, x/c=0.80 porous LEX, x/c=0.80

Fig. 5. Vapor screen flow visualization of solid and porous LEX configurations at Mach=1.6, α=8°

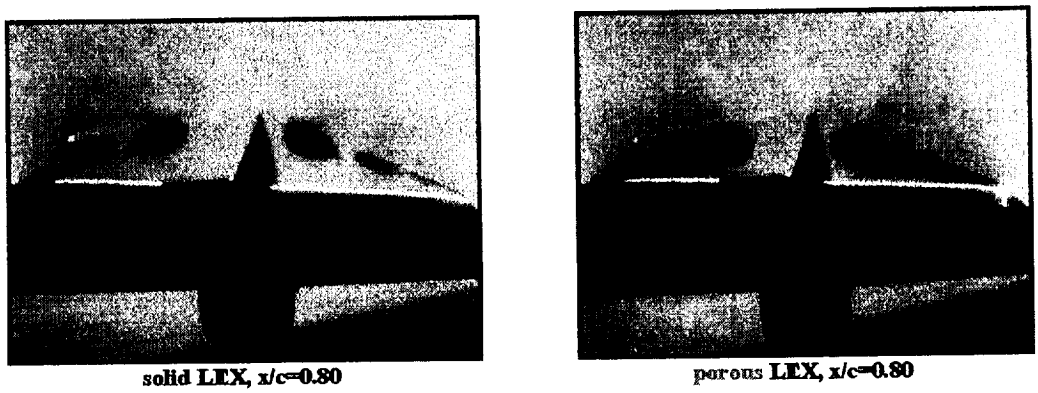

solid LEX, x/c=0.80 porous LEX, x/c=0.80

Fig. 6. Vapor screen flow visualization of solid and porous LEX configurations at Mach=2.1, α=12°

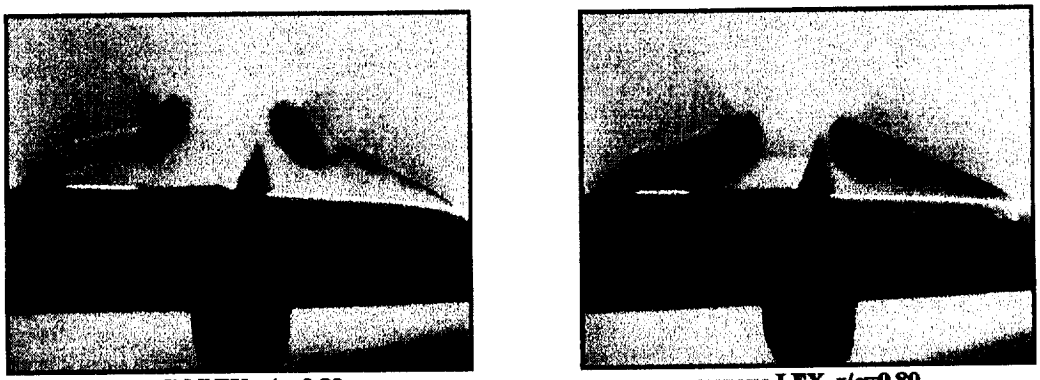

solid LEX, x/c=0.80 porous LEX, x/c=0.80

Fig. 7. Vapor screen flow visualization of solid and porous LEX configurations at Mach=2.1, α=16°

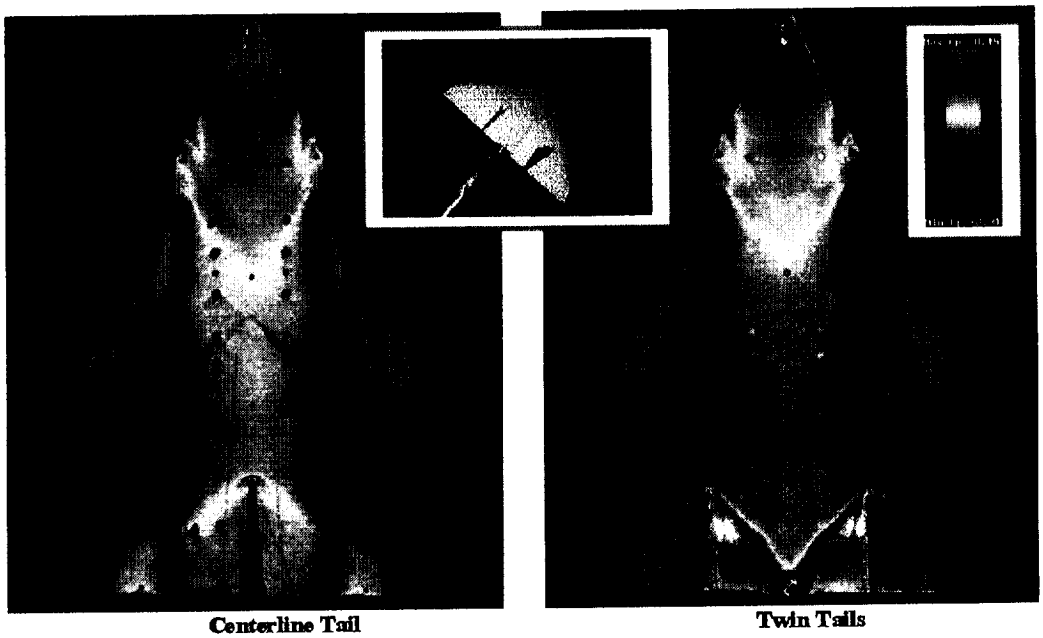

Centerline Tail Twin Tails

Fig. 8. Comparison of PSP intensity field images with centerline and twin vertical tails at Mach=1.6, α=8° (color-coded pressure coefficient range +0.16 (red/pink) to –0.31 (blue/purple))

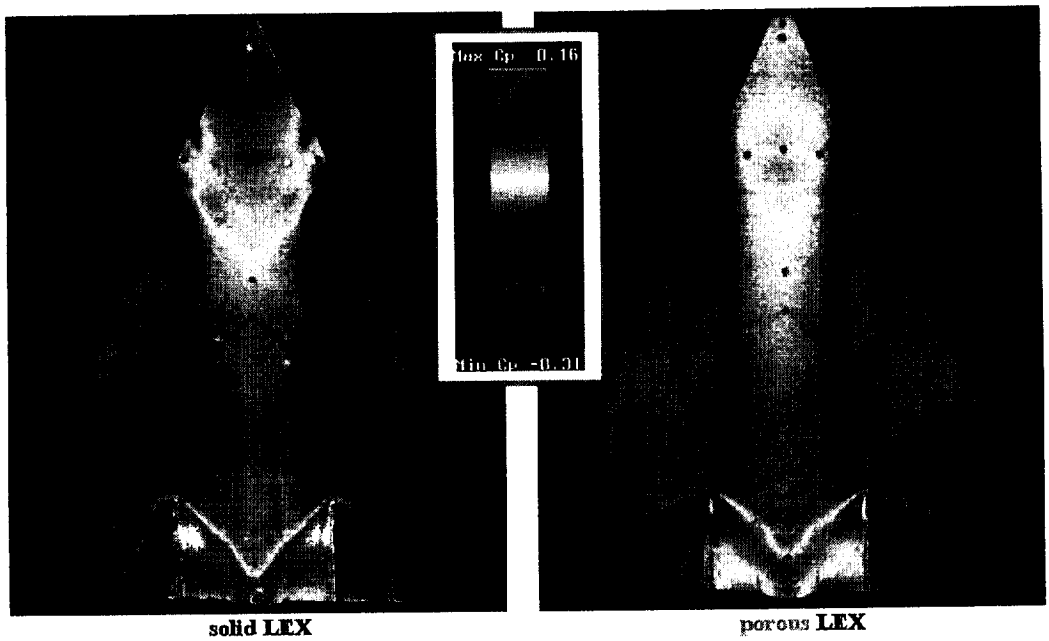

Fig. 9. Comparison of PSP intensity field images with solid and porous LEX at Mach=1.6, α=8° (color-coded pressure coefficient range +0.16 (red/pink) to –0.31 (blue/purple))

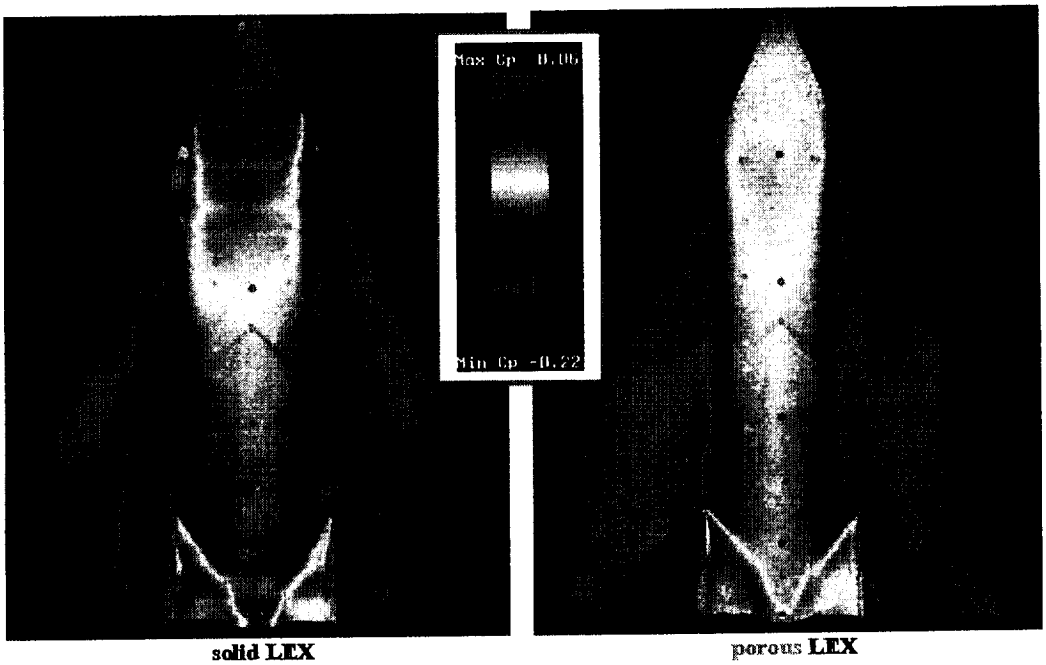

Fig. 10. Comparison of PSP intensity field images with solid and porous LEX at Mach=2.1, α=8° (color-coded pressure coefficient range +0.06 (red/pink) to –0.22 (blue/purple))

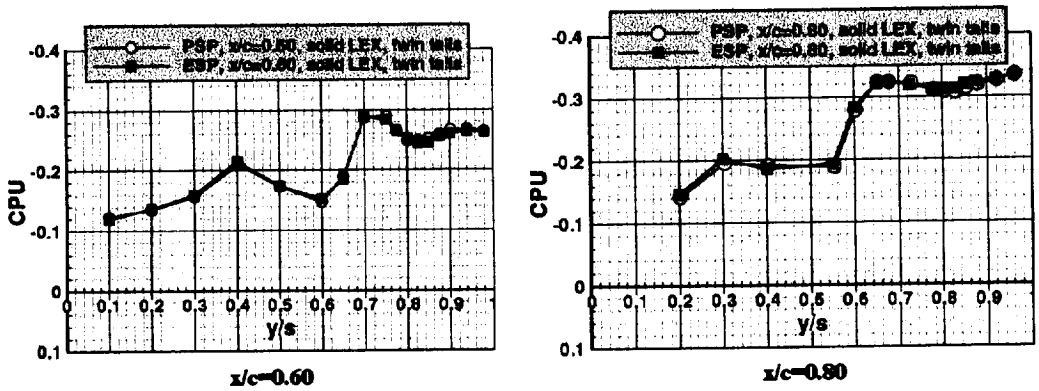

Fig. 11. Comparison of PSP and ESP pressure distributions at Mach=1.6, α=8°

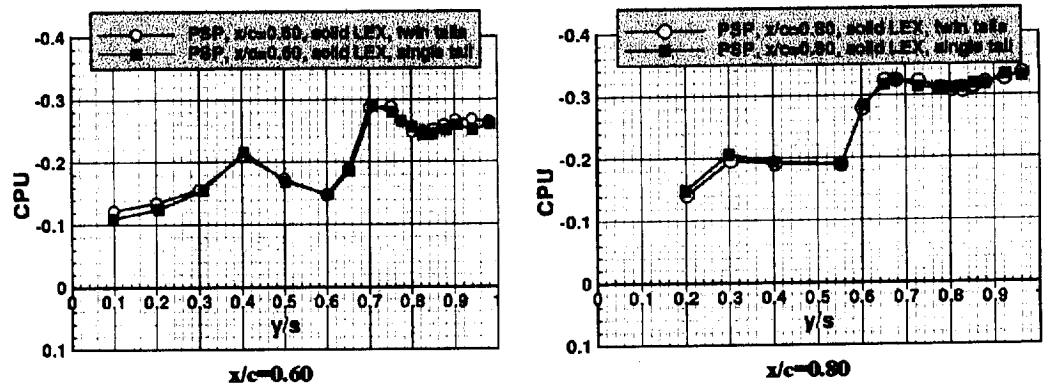

Fig. 12. Comparison of PSP pressure distributions with centerline and twin tails at Mach=1.6, α=8°

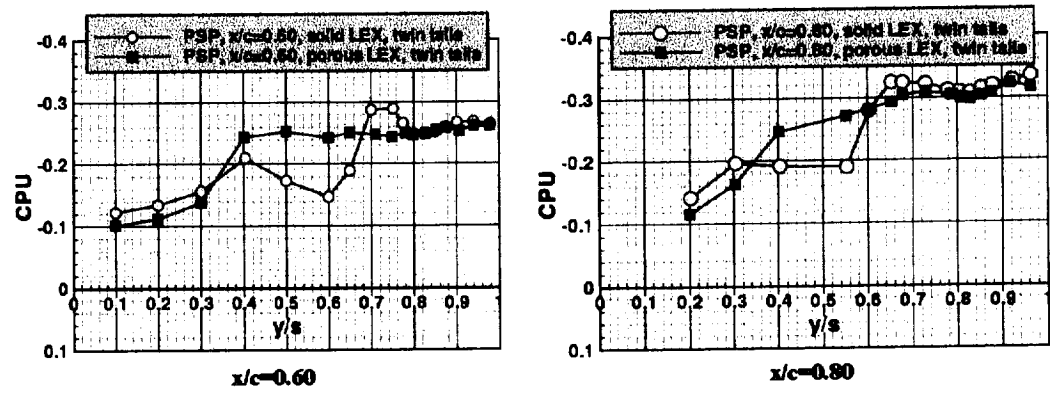

Fig. 13. LEX porosity effect on PSP pressure distributions at Mach=1.6, α=8°

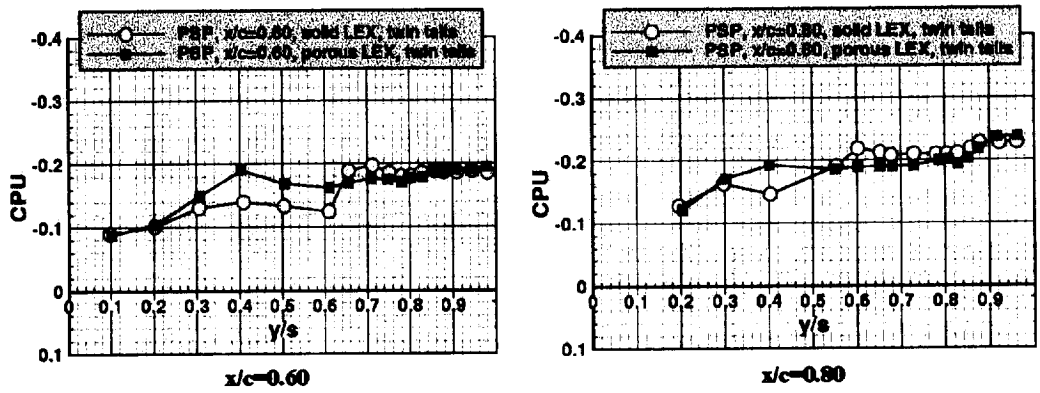

Fig. 14. LEX porosity effect on PSP pressure distributions at Mach=2.1, α=8°

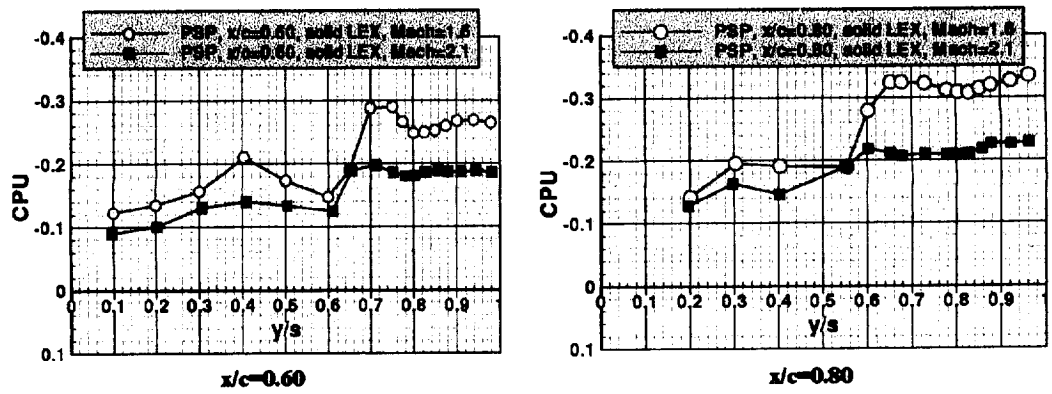

Fig. 15. Mach number effect on PSP pressure distributions at α=8°, solid LEX

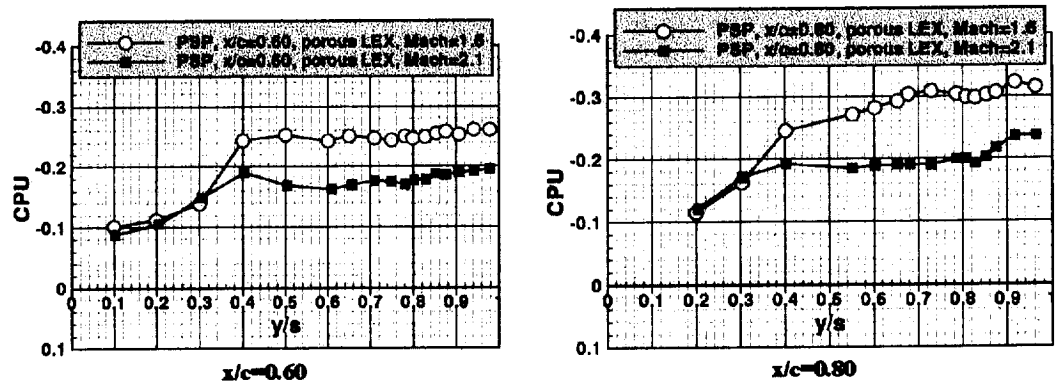

Fig. 16. Mach number effect on PSP pressure distributions at α=8°; porous LEX